Isotropic Turbulence: Important Differences between True Dissipation Rate and Its One-Dimensional Surrogate

Iwao Hosokawa and Shin-ichi Oide
University of Electro-Communications, Chofu, Tokyo 182, Japan

Kiyoshi Yamamoto
National Aerospace Laboratory, Chofu, Tokyo 182, Japan
(Received 5 February 1996; revised manuscript received 8 July 1996)

The one-dimensional surrogate (1D) of energy dissipation rate has often been used in place of the true one in investigations of the Kolmogorov refined similarity hypothesis and the multifractal nature of isotropic turbulence. Direct numerical simulations, reported here, show that the use of the 1D surrogate can lead to fundamental changes in statistics. The conditional and unconditional probability densities of the Kolmogorov variable built from the true dissipation are never bimodal and always nearly Gaussian. [S0031-9007(96)01772-3]

PACS numbers: 47.27.Gs, 05.40.+j, 05.70.Ln

Many experimenters have measured the so-called pseudodissipation rate $\varepsilon' = 15\nu(\partial u/\partial x)^2$ (ν: kinematic viscosity, $\partial u/\partial x$: longitudinal velocity gradient), that is the one-dimensional (1D) surrogate of energy dissipation rate ε in isotropic turbulence. This is done instead of measuring ε directly because it is hard to measure all the simultaneous components of the strain tensor. In most cases discussions of intermittency exponents have been based on observations of the surrogate ε' with the use of the Taylor hypothesis. In particular, it is to be remarked that several current important ideas on the fine structure of turbulence, such as the multifractal distribution of dissipation in space [1] and the bimodality of conditional probability density functions (PDF) for a small scale range [2] of the Kolmogorov variable in the refined similarity hypothesis (RSH) [3], have been established by analysis based on ε'.

However, the true ε may give important different results. This possibility has already been pointed out [4–7]. Here we compare results obtained by constructing ε and ε' from two direct numerical simulations (DNS) of fully developed, decaying isotropic turbulence at $R_\lambda \sim 100$ [8] and $R_\lambda \sim 160$ [9]. Here R_λ is a Taylor-scale Reynolds number. The grid sizes were 128^3 and 512^3, respectively. The method of calculation was described in [10].

First we show in Fig. 1(a) the unconditional PDF's of the Kolmogorov variable v defined by the RSH [3] for various fixed scales r:

$$\Delta u_r = v(r\varepsilon_r)^{1/3}, \tag{1}$$

where Δu_r is longitudinal velocity increment across distance r, and ε_r is ε averaged over a domain of scale r. We take the domain as a cube with side r, between the centers of opposite faces of which the Δu_r is measured. v is normalized by its root mean square. These PDF's have skewness at most -0.3 but are very close to Gaussian, with a slight r dependence. In contrast, we show in Fig. 1(b) the corresponding results with the surrogate dissipation ε'_r used in place of ε_r. In this case ε'_r is defined as the average of ε' over a line of length r across which Δu_r is measured. These PDF's appear to be bimodal for small r and gradually become more Gaussian as r increases. These data in Fig. 1 are the computation for $R_\lambda \sim 160$; nine cases of r are plotted ranging from 1.16 to 298 Kolmogorov lengths η, so that the inertial range covers $r/\eta = 18.58$ and 37.2, and $r/\eta = 9.28$ is just at the end of it.

Note that the inertial range in the DNS of Wang *et al.* [11], who treat forced isotropic turbulence by Fourier spectral method, starts at $r/\eta \cong 10$, corresponding to $k\eta = 0.3$ where k is the wave number. This rather

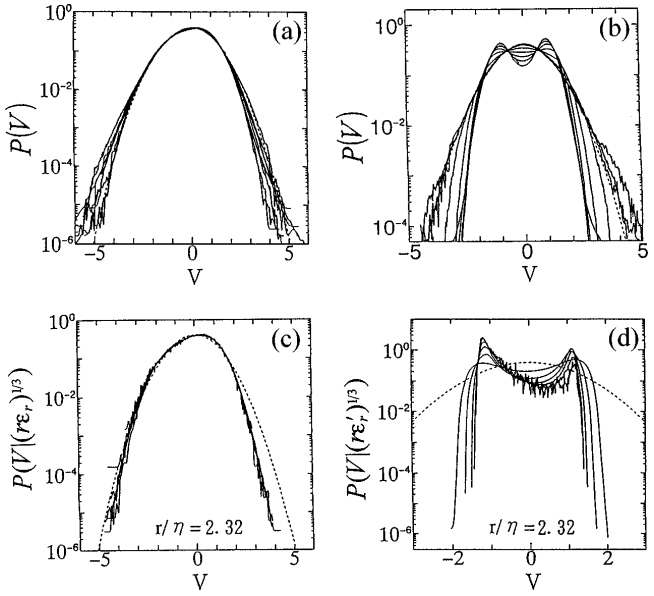

FIG. 1. The unconditional PDS'f of v for various r for (a) the true dissipation and (b) its 1D surrogate; $r/\eta = 1.16$, 2.32, 4.64, 9.29, 18.58, 37.2, 74.3, 149, and 298. As r/η increases, the line moves to the outside. The conditional PDF's of v for $r/\eta = 2.32$ for several values of (c) $(r\varepsilon_r)^{1/3}$ and (d) $(r\varepsilon'_r)^{1/3}$. As $(r\varepsilon'_r)^{1/3}$ increases, the line moves to the inside. The dotted lines denote the standard normal PDF.

 0031-9007/96/77(22)/4548(4)$10.00

small value of r/η at the end is common to existing DNS of isotropic turbulence.

The bimodality seen in Fig. 1(b) is very similar to that of the conditional PDF's of v for the surrogate dissipation, which were depicted in detail by Stolovitzky *et al.* [2] based on the experimental observation of real turbulence in an atmospheric surface layer with $R_\lambda \sim 1500$ and 2000. Since we are interested in the existence or nonexistence of bimodality, first we show the conditional PDF's of v for ε_r and ε_r' for a small r ($r/\eta = 2.32$) in Figs. 1(c) and 1(d). It is evident that there is no bimodality found in the conditional PDF's of v for ε_r even for such a small r for any $(r\varepsilon_r)^{1/3}$. The PDF hardly depends on $(r\varepsilon_r)^{1/3}$. On the other hand, that for ε_r' is clearly bimodal and strongly depends on $(r\varepsilon_r')^{1/3}$; the more bimodal for the larger $(r\varepsilon_r')^{1/3}$. All lines are drawn for a value zone of $(r\varepsilon_r)^{1/3}$ or $(r\varepsilon_r')^{1/3}$ which is one of the octad made by dividing the whole zone between the maximum and minimum of $(r\varepsilon_r)^{1/3}$ or $(r\varepsilon_r')^{1/3}$ into eight equal parts, only when each zone has a sufficient number of data points to draw a line. Ruggedness of lines means that the data number is relatively small, and it happens usually when $(r\varepsilon_r)^{1/3}$ or $(r\varepsilon_r')^{1/3}$ is large but also when it is very small for large r. In Fig. 1(d), however, we notice that the transition pattern of the conditional PDF with $(r\varepsilon_r')^{1/3}$ is the reverse of what was presented in [2] and resembles a *persistent case* of the process treated in [12]. As $(r\varepsilon_r')^{1/3}$ increases, the line moves from outside to inside. This pattern implies the fractional Brownian motion with Hurst number $H > \frac{1}{2}$, being consistent with the fact that $\Delta u_r \sim r$ for $r \to 0$ due to analyticity; whence $H \to 1$.

We show the same comparisons for $r/\eta = 9.29$ and 18.58 in Fig. 2. Figures 2(a) and 2(c) identify the tendency which appeared in Fig. 1(c) and the more Gaussianization of the PDF but holding a skewness. In Fig. 2(b) we can see that the conditional PDF for ε_r' still keeps the bimodality for smaller $(r\varepsilon_r')^{1/3}$, but the transition pattern is now similar to that in [2]. That is, these PDF's resemble an *antipersistent case* [12] corresponding to the fractional Brownian motion with $H < 1/2$, as is expected in the inertial range. Figure 2(d) has the same trend, but the conditional PDF's for larger $(r\varepsilon_r')^{1/3}$ are closer to Gaussian. As r increases beyond the values shown here, we have made sure that the conditional PDF for the true dissipation approaches to more Gaussian irrespectively of $(r\varepsilon_r)^{1/3}$, while that for the surrogate does so considerably depending on $(r\varepsilon_r')^{1/3}$ even in the inertial range (faster for larger $(r\varepsilon_r')^{1/3}$) just as is presented in [2].

Thus it is natural to conclude that the bimodality is peculiar to the PDF of v for the surrogate dissipation, and that the PDF of v for the true dissipation may be assumed as nearly Gaussian for a wide range of r (down to the scale of η) and is hardly conditioned by $(r\varepsilon_r)^{1/3}$, but slightly dependent on r [13]. For reference, we show the skewness and kurtosis of the unconditional PDF of

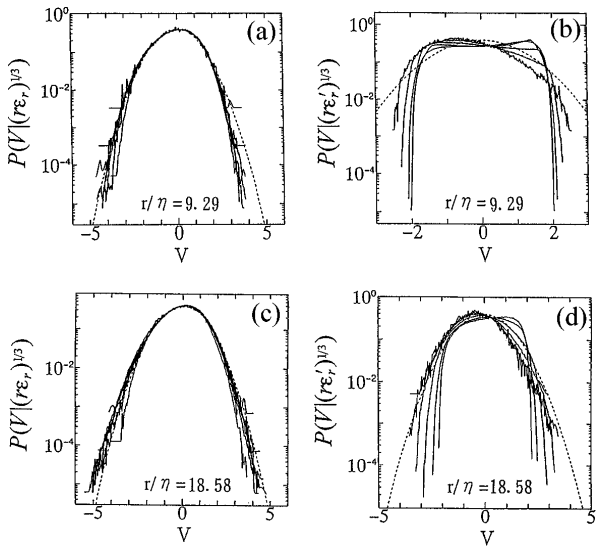

FIG. 2. The conditional PDF's of v for $r/\eta = 9.29$ for several values of (a) $(r\varepsilon_r)^{1/3}$ and (b) $(r\varepsilon_r')^{1/3}$, and these for $r/\eta = 18.58$ for several values of (c) $(r\varepsilon_r)^{1/3}$ and (d) $(r\varepsilon_r')^{1/3}$. As $(r\varepsilon_r')^{1/3}$ increases, the line moves to the outside in both (b) and (d). The dotted lines denote the standard normal PDF.

v for the true dissipation against r/η in Fig. 3. An appreciable dependence of the kurtosis on r is seen even in the inertial range (shown by arrows in Fig. 3). The trend of the kurtosis decreasing as r decreases in the inertial range is clearly seen also in the experiments for $R_\lambda = 550$ [14] and $R_\lambda = 7200$ [15]. This may reveal a small gap between reality and the RSH that assumes the perfect independence of the PDF of v of both r and $(r\varepsilon_r)^{1/3}$ in the inertial range.

By the way, we note that the ensemble average of unnormalized v^3, say $\langle v^3 \rangle$, in the inertial range is just around -1, which roughly approximates $-\frac{4}{5}$ in the Kolmogorov theory [16]:

$$\langle \Delta u_r^3 \rangle = -\tfrac{4}{5} r \langle \varepsilon_r \rangle . \qquad (2)$$

Note that v is almost independent of $(r\varepsilon_r)^{1/3}$ for the true dissipation. This may indicate a limit of simulation of the ideal state ($R_\lambda \to \infty$) which can be achieved by our DNS turbulence. On the other hand, noting that

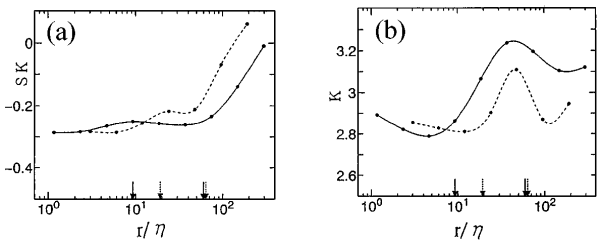

FIG. 3. (a) Skewness and (b) kurtosis of PDF of v for the true dissipation against r/η for $R_\lambda \sim 160$ (solid line) and $R_\lambda \sim 100$ (dotted line). The inertial range of each case is in between the arrows.

$\langle \Delta u_r^2 \rangle = \langle v^2 \rangle \langle \varepsilon_r^{2/3} \rangle r^{2/3}$, we obtained about 2.7 as the value of $\langle v^2 \rangle$ in the inertial range. After multiplying it by $\frac{55}{27}\Gamma^{-1}(1/3)$ [17], we have the Kolmogorov constant C_K for our turbulence as 2.1, the same value as in [10]. The intermittency effect for $\langle \varepsilon_r^{2/3} \rangle$ is negligible here. This rather high value of C_K is common to current DNS's of turbulence.

Stolovitzky and Sreenivasan [12] succeeded in deriving theoretically the conditional PDF of v for the surrogate by utilizing the special analytical relationship of Δu_r and $r\varepsilon_r'$ established using the 1D common function $\partial u/\partial x$ and with some assumptions. That is bimodal for small r and approaches to Gaussian for larger r in rather excellent agreement with their experimental observation using the surrogate, but without any skewness. We can understand the source of appearance of the bimodality very well from their theory, and have actually reconfirmed it in our DNS only when ε_r' replaces ε_r. However, the PDF of v for the true dissipation is not really bimodal all the way down to $r \approx \eta$ but nearly Gaussian, in contrast. On the other hand, RSH is originally based on the similarity concept employing the true dissipation. Therefore it is natural to understand the statistics of Δu_r as a joint result of the nearly Gaussian statistics of v and the proper statistics of $(r\varepsilon_r)^{1/3}$, as in literature mentioned in Ref. [13]. Stolovitzky *et al.*'s theory of v hardly contributes to this even in the inertial range. Indeed it is a problem that the PDF of v in their theory is not skewed in the inertial range, since there is no other source to produce the real skewness of the PDF of Δu_r in the relation (1). The crucial dynamic role in turbulence of the skewness was well described by Kolmogorov [16]. As a result, it must be difficult to generate real Δu_r based on their theory.

In Fig. 4, we compare the generalized dimensions $D(q)$'s obtained for the surrogate measure and for the true dissipation measure. Here we understand that the former gives a multifractal in the 1D space (or a 1D cut of the 3D space). So let us distinguish it as $D(q)^{(1)}$ from $D(q)$ in the 3D space. Since we have many lines of total length L (in the x direction) in the DNS box of turbulence, we can get many $D(q)^{(1)}$'s calculated in every line by the box counting method [18]. These $D(q)^{(1)}$'s scatter just as wildly as in the experiment by Meneveau and Sreenivasan [19]. Then, together with these authors who contrived the p model by averaging the scattered data, we may consider the $D(q)^{(1)}$ averaged over all of 128^2 $D(q)^{(1)}$'s for $R_\lambda \sim 100$ as the most significant. Our averaged $D(q)^{(1)}$ is shown by closed diamonds in the Figure. The p model [1] is indicated by the dashed line. Open squares show the case where L is replaced by the inertial-range length $L/8$. Note that we have set $D(q) = D(q)^{(1)} + 2$ as the 3D version of the multifractal [1]. From the figure we may judge that our DNS supports the p model substantially as expected, only if the surrogate is treated in the 1D space. On the other hand, the $D(q)$'s for the true dissipation (by the 3D box counting method)

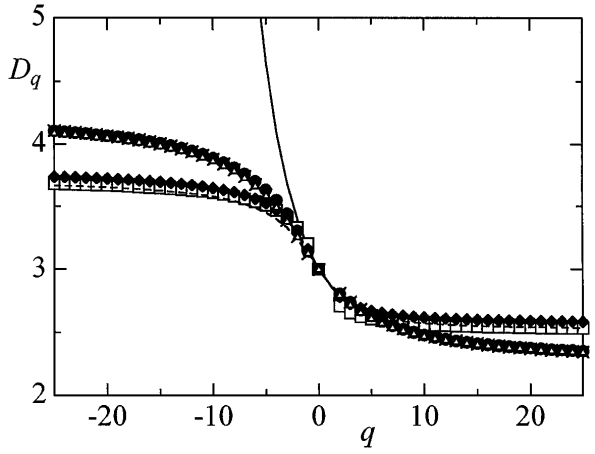

FIG. 4. Comparison of generalized dimensions $D(q)$. The DNS values for $R_\lambda \sim 160$ are indicated by closed circles, those for $R_\lambda \sim 100$ by crosses, and $D(q)$ for the trinomial generalized Cantor set model by open triangles. $D^{(1)}(q) + 2$ for the p model is indicated by the dashed line, the average $D^{(1)}(q) + 2$ for the 1D surrogate dissipation for $R_\lambda \sim 100$ by closed diamonds, and the She-Leveque model by the solid line, which almost overlaps with closed circles, crosses, and open triangles for $q \geq 0$. Open squares indicate the average $D^{(1)}(q) + 2$ when the box counting is done for the inertial-range length $L/8$ in place of L.

are plotted by closed circles and crosses for $R_\lambda \sim 160$ and 100, respectively. These are close to each other, suggesting the robustness of $D(q)$ of the multifractal of dissipation measure in the 3D space.

To demonstrate how reliable the scaling of $D(q)$ by the box counting for a deterministic multifractal [18] is, we add Fig. 5 in which $\ln[\Sigma_i (E_r^{(i)}/E_L)^q]^{1/(q-1)}$ (where $E_r = \varepsilon_r r^3$) is plotted against $\ln(r/L)$. There we can see a good scaling exist for a much wider than the inertial range. See [20] for the detailed investigation of scaling with 29 plotted points straightly aligned inside the inertial range for $R_\lambda \sim 100$. The scaling of the averaged $D(q)^{(1)}$ is shown in the same figure by open symbols in comparison.

Thus we can conclude that there is a non-trivial difference in $D(q)$ between the surrogate and the true dissipation. Only for $|q| < 3$ both $D(q)$'s are almost coincident. We may understand that the p model extracted from $D(q)^{(1)}$ will play a good role in treating a nature of turbulence relevant to only low-order moments of Δu_r in the inertial range. This fact, actually found in Fig. 1 in [21], is now reconfirmed by the additional data obtained by the higher-resolution device.

The trinomial generalized Cantor set model [22] was contrived to improve the previously published 3D binomial Cantor set model [21]. The intermittency exponents for that model is expressed as

$$\mu(q) = \log_A(\nu_1 B^q + \nu_2 M^q + \nu_3 C^q), \qquad (3)$$

where $A = 1.45214$, $B = 1.32284$, $M = 1.04693$, $C = 0.62732$, $\nu_1 = 0.326569$, $\nu_2 = 0.346863$ and

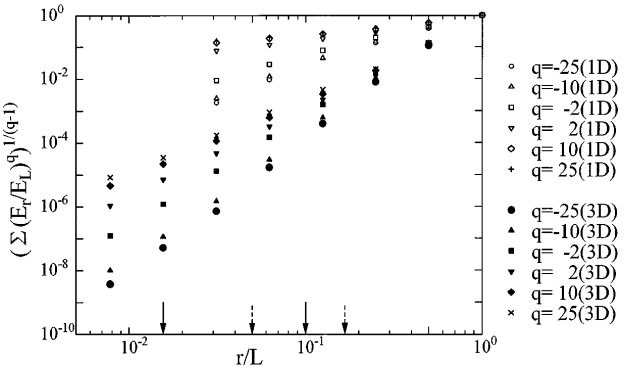

FIG. 5. $[\Sigma_i(E_r^{(i)}/E_L)^q]^{1/(q-1)}$ vs r/L and $[\Sigma_i(E_r^{\prime(i)}/E_L^{\prime})^q]^{1/(q-1)}$ vs r/L. The main box of side L for the case of $R_\lambda \sim 160$ is split into 8^n subboxes of side $r = L/2^n$; n runs from one to seven, avoiding the dissipation range. $D(q)$ was determined as the slope of the best-fit line for the seven points for each q rather than for the three in the inertial range indicated by the arrows, just as done in [8], since the scaling is so well observed much beyond the inertial range. In comparison, $[\Sigma_i(E_r^{\prime(i)}/E_L^{\prime})^q]^{1/(q-1)}$ averaged over 128^2 samples vs r/L to calculate the averaged $D^{(1)}(q)$ are plotted by open symbols. $D^{(1)}(q)$ was determined as the slope of the best-fit line for six points in the figure similarly. This process is mathematically equivalent to the averaging 128^2 $D^{(1)}(q)$'s separately calculated from each sample.

$\nu_3 = 0.326569$. The generalized dimensions are simply related with the intermittency exponents like $D(q) = -\mu(q)/(q-1) + 3$ [23]. The $D(q)$ obtained from (3) is indicated by open triangles in Fig. 4 in excellent agreement with the DNS in the entire region. We add in the figure the She-Leveque model [24] which has intermittency exponents:

$$\mu(q) = 2q/3 - 2[1 - (2/3)^q]. \qquad (4)$$

This model, indicated by the solid line, is remarkably close to our DNS and the trinomial generalized Cantor set model only for $q \geq 0$. But it blows up even more rapidly for $q < 0$ than the lognormal model [3]; it is well known that the lognormal model yields the straight line tangent to both Cantor set models at $q = 0$ [8,21] when the same value of $\mu(2)$ is taken. This suggests that the She-Leveque model has a weakpoint in describing the multifractal nature of weak dissipation. $D(q)$'s for many other models were compared in [25].

In conclusion, we disclosed important differences between the true dissipation rate and its 1D surrogate in isotropic turbulence, by treating the PDF of v and the multifractal nature of dissipation on the basis of our DNS data. Chen *et al.* [26] addressed no qualitative difference between both in the treatment of conditional average of $|\Delta u_r|$, but they did not analyze such detailed features as treated here. On the other hand, Wang *et al.* [11] found a large difference in some aspect related to RSH between both. Our result makes the detail of the difference much clearer. Even though the R_λ reached by the DNS is still low as compared with that by experiment, the present result indicates a need to reconsider any induction based only on the knowledge from the 1D surrogate dissipation.

We thank Bob Kraichnan for his useful advice and T. Satoh for his computational assistance.

[1] C. Meneveau and K. R. Sreenivasan, Phys. Rev. Lett. **59**, 1424 (1987).
[2] G. Stolovitzky, P. Kailasnath, and K. R. Sreenivasan, Phys. Rev. Lett. **69**, 1178 (1992).
[3] A. N. Kolmogorov, J. Fluid Mech. **13**, 82 (1962).
[4] R. Narasimha reports Roger and Moin's (1987) result in *Turbulence at the Cross Roads*, edited by J. L. Lumley (Springer, Berlin, 1990), p. 13.
[5] A. Tsinober, E. Kit, and T. Dracos, in *Advances in Turbulence 3*, edited by A. V. Johansson and P. H. Alfredsson (Springer, Heidelberg, 1991), p. 514.
[6] I. Hosokawa, J. Phys. Soc. Jpn. **64**, 3141 (1995).
[7] S. T. Thoroddsen, Phys. Fluids **7**, 691 (1995).
[8] I. Hosokawa and K. Yamamoto, J. Phys. Soc. Jpn. **59**, 401 (1990); Phys. Fluids A **2**, 889 (1990); in *Turbulence and Coherent Structures*, edited by O. Metais and M. Lesieur (Kluwer, Dordrecht, 1991), p. 177.
[9] K. Yamamoto, I. Hosokawa, and K. Sakai, Res. Inst. Math. Sci. Rep. **892**, 217 (1995); K. Yamamoto, Nagare **14**, 353 (1995).
[10] K. Yamamoto and I. Hosokawa, J. Phys. Soc. Jpn. **57**, 1532 (1988).
[11] L.-P. Wang, S. Chen, J. G. Brasseur, and J. C. Wyngaard, J. Fluid Mech. **309**, 113 (1996).
[12] G. Stolovitzky and K. R. Sreenivasan, Rev. Mod. Phys. **66**, 229 (1994).
[13] This validates the treatment of the PDF and scaling nature of velocity increment in I. Hosokawa, J. Phys. Soc. Jpn. **62**, 3792 (1992); Phys. Rev. E **51**, 781 (1995); Fluid Dyn. Res. **15**, 337 (1995); J. Phys. Soc. Jpn. **64**, 3141 (1995).
[14] I. Hosokawa, C. W. Van Atta, and S. T. Thoroddsen, Fluid Dyn. Res. **13**, 329 (1994).
[15] Y. Zhu, R. A. Antonia, and I. Hosokawa, Phys. Fluids **7**, 1637 (1995).
[16] A. N. Kolmogorov, Dokl. Acad. Nauk USSR **30**, 301 (1941);**32**, 19 (1941).
[17] A. S. Monin and A. M. Yaglom, *Statistical Fluid Mechanics* (MIT, Cambridge, Massachusetts, 1975), Vol. 2, p. 355.
[18] T. C. Halsey, M. H. Jensen, L. P. Kadanoff, I. Procaccia, and B. I. Shraiman, Phys. Rev. A **33**, 1141 (1986).
[19] C. Meneveau and K. R. Sreenivasan, Nucl. Phys. B (Proc. Suppl.) **2**, 49 (1987).
[20] I. Hosokawa and K. Yamamoto, Phys. Fluids A **2**, 889 (1990).
[21] I. Hosokawa, Phys. Rev. Lett. **66**, 1054 (1991).
[22] I. Hosokawa, S. Oide, and K. Yamamoto, J. Phys. Soc. Jpn. **65**, 873 (1996).
[23] I. Hosokawa, Proc. R. Soc. London A (to be published).
[24] Z.-S. She and E. Leveque, Phys. Rev. Lett. **72**, 336 (1994).
[25] I. Hosokawa, J. Phys. Soc. Jpn. **62**, 3347 (1993).
[26] S. Chen, G. D. Doolen, R. H. Kraichnan, and Z.-S. She, Phys. Fluids A **5**, 458 (1993).